Geochemical Perspectives Letters

Iron(III) reducing bacteria immobilise antimonite by respiring elemental sulfur

L. Ye[1], C. Jing[1,2*]

OPEN ACCESS

https://doi.org/10.7185/geochemlet.2215

Abstract

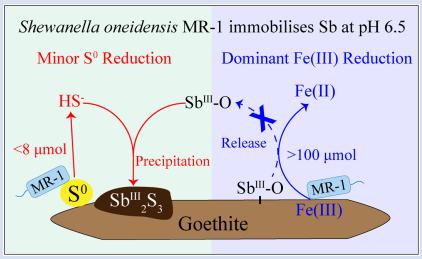

Iron(III) reducing bacteria (IRB) are best known and most influential drivers for mobilising metal(loid)s *via* reductive dissolution of iron(III)-containing minerals. Our study challenges this preconception and found that IRB immobilise metal(loid)s by respiring elemental sulfur (S^0) even when Fe(III) reduction is prevailing under mildly acidic conditions. Antimony (Sb), a toxic contaminant, was chosen as an example of metal(loid)s. Antimonite-adsorbed goethite was incubated with *Shewanella oneidensis* MR-1, a widely distributed IRB, in the presence of S^0 at pH 6.5. The results show that although the extent of Fe(III) reduction (>100 µmol) was over ten times greater than that of S^0 reduction (<8 µmol), it was S^0 reduction that immobilised Sb through Sb_2S_3 precipitation. Further, the thermodynamic calculation suggests that such great impacts of marginal S^0 reduction can be extended to other metal(loid)s *via* the formation of soluble thio-species or sulfide precipitates. This study redefines the role of IRB in the environmental fate of metal(loid)s, highlighting the strong impacts from the marginal S^0 reduction over the central Fe(III) reduction.

Received 23 December 2021 | Accepted 3 March 2022 | Published 5 May 2022

Introduction

Iron oxides are natural scavengers for toxic metal(loid)s and iron reducing bacteria (IRB) mobilise these metal(loid)s by facilitating the reductive dissolution of iron oxides (Kappler *et al.*, 2021). For example, elevated arsenic (As) (Kontny *et al.*, 2021), antimony (Sb) (Hockmann *et al.*, 2014), mercury (Hg) (Wang *et al.*, 2021) and cadmium (Cd) (Zhou *et al.*, 2020) in waters usually associate with increasing Fe(II) concentrations in the presence of IRB. In fact, many IRB, such as *Shewanella* and *Geobacter* spp., have an underappreciated ability: elemental sulfur (S^0) respiration (Flynn *et al.*, 2014). Accordingly, the biogenic sulfide (HS^-) may either immobilise metal(loid)s *via* sulfide precipitates or mobilise them by forming soluble thio-species (Planer-Friedrich *et al.*, 2020; Ye *et al.*, 2020; Helz, 2021). Previous studies suggested that S^0 is widely distributed in sediments and waters, and its concentration can be as high as 60 mM as summarised in Table S-1. S^0 usually co-exists with Fe(III) oxides in the environment where FeS oxidation occurs (Burton *et al.*, 2009) or where microbial sulfate reduction occurs in the presence of Fe(III) oxides (Burton *et al.*, 2011). Thus, rather than Fe(III) reduction alone, IRB influence the mobility of metal(loid)s *via* coupled Fe(III) and S^0 reduction.

The extents of Fe(III) and S^0 reduction reveal their contribution in regulating the fate of metal(loid)s. Our recent work found that IRB prefer to reduce S^0 under mildly alkaline conditions, and the biogenic sulfide greatly enhanced Sb release by the formation of thioantimonates (Ye *et al.*, 2022). In contrast, in the acidic environments, IRB prefer to respire Fe(III) rather than S^0 to conserve more energy (Flynn *et al.*, 2014). The effect of S^0 respiration by IRB is previously neglected and probably masked by appreciable Fe(III) reduction on the fate of metal(loid)s. Thus, prevailing Fe(III) reduction (Cummings *et al.*, 2000) is commonly considered to drive the mobility of metal(loid)s in mildly acidic sediments (Hockmann *et al.*, 2015), such as mining areas and acidic wetlands (Karimian *et al.*, 2018).

Contrary to the previous preconception, our study revealed that S^0 respiration by IRB even to a marginal extent can greatly shape the fate of metal(loid)s under mildly acidic conditions. In detail, antimony (Sb), an emerging contaminant, is chosen as an example of metal(loid)s. Antimonite-adsorbed goethite was incubated with *Shewanella oneidensis* MR-1, a typical Fe(III) reducing bacterium, in the presence of S^0 at pH 6.5. Our incubation and characterisation results suggest that although Fe(III) was the dominant electron acceptor and Fe(III) reduction was over ten times greater than S^0 reduction, Sb release was mainly inhibited by biogenic sulfide through the formation of Sb_2S_3 precipitates. The thermodynamic calculation further indicates that the strong effect of marginal S^0 reduction can be extended from Sb to other metal (loid)s. This study breaks the stereotype that IRB influence the mobility of metal(loid)s *via* Fe(III) reduction alone, and highlights the importance of S^0 respiration.

Materials and Methods

The experiments were performed at pH 6.5 in the dark, and the experimental setup and analytical techniques were similar to our previous study (Ye *et al.*, 2022). Dissolved Fe(II), sulfide,

1. Shandong Key Laboratory of Environmental Processes and Health, School of Environmental Science and Engineering, Shandong University, Qingdao 266237, China
2. State Key Laboratory of Environmental Chemistry and Ecotoxicology, Research Center for Eco-Environmental Sciences, Chinese Academy of Sciences, Beijing 100085, China
* Corresponding author (email: cyjing@rcees.ac.cn)

antimonite, antimonate and thioantimonates were analysed periodically during the incubation. To extend the effect of marginal S^0 reduction from Sb to other metal(loid)s, reaction path models were established to calculate the species of Sb, arsenic (As), tungsten (W), molybdenum (Mo), mercury (Hg), lead (Pb), zinc (Zn), cadmium (Cd) and copper (Cu) as a function of pH and the activity of sulfide in the presence of goethite. More details of the methods are shown in the Supplementary Information (SI).

Results and Discussion

Prevalent Fe(III) reduction versus minor S^0 reduction. During the incubation with *Shewanella oneidensis* MR-1 at pH 6.5 (Fig. S-2), the electron donor was formate and the electron acceptor was either goethite or S^0. To determine the dominant electron acceptor in our experiments, dissolved Fe(II) and sulfide (HS^-) were measured (Fig. 1) and the electrons accepted by goethite or S^0 were calculated (Table S-2). In the abiotic control without MR-1 (Goe-Sb^{III}+S^0), Fe(II) and sulfide were not detected (Fig. 1). In the presence of MR-1 (MR-1+Goe-Sb^{III}+S^0), dissolved Fe(II) concentrations reached up to 527 ± 27 μM whereas sulfide was below 3 μM during the 192 hr incubation (Fig. 1a). Such a low sulfide concentration (<3 μM) would have a negligible effect on goethite reduction (Poulton *et al.*, 2004). At the end of incubation, 2.7 ± 0.5 μmol/g Fe(II) were adsorbed on solids and 26.6 ± 3.4 μmol/g sulfide were precipitated (Table S-2). Overall, goethite accepted 106.1 ± 5.3 μmol electrons from MR-1 while S^0 accepted 14.4 ± 1.6 μmol. The order of magnitude difference in electrons suggested that goethite was the dominant electron acceptor at pH 6.5.

Consistent with the prevailing Fe(III) reduction, the thermodynamic calculations show that the free energy gain (ΔG_r) with goethite as the electron acceptor is higher than that with S^0 (Fig. S-3), as detailed in SI. Previous studies also suggested that microbial Fe(III) reduction is the central pathway in acidic environments under anoxic conditions, and IRB are the dominant bacteria therein (Sun *et al.*, 2015). Inconsistent with the redox ladder concept (Peiffer *et al.*, 2021), minor S^0 reduction still occurred although in a lower ΔG_r than goethite. However, no research has paid attention to the marginal S^0 reduction by IRB in acidic environments.

Minor S^0 reduction immobilises Sb. As a primary pathway, Fe(III) reduction has been reported to enhance Sb release due to a depletion of sorption sites (Hockmann *et al.*, 2014); however, the concentration of total dissolved Sb decreased from 9.07 ± 0.48 μM to 0.19 ± 0.07 μM in MR-1+Goe-Sb^{III}+S^0 (Fig. 1b). In the abiotic control (Goe-Sb^{III}+S^0; Fig. 1c), the Sb concentration slightly increased from 7.33 ± 0.27 μM to 8.95 ± 0.57 μM during the incubation. The dissolved Sb was mainly Sb^{III}-O, and no thiolated Sb species was detected by IC-ICP-MS (Fig. 1b-c). The decrease in dissolved Sb in MR-1+Goe-Sb^{III}+S^0 was consistent with the loss of Sb^{III}-O (Fig. 1b).

The loss of dissolved Sb^{III}-O in MR-1+Goe-Sb^{III}+S^0 was due to the formation of Sb_2S_3 as evidenced by Sb L_I-edge XANES analysis (Figs. 2a, S-4 and Table S-4). In detail, the first derivative peak at 4703 eV in Goe-Sb^{III}+S^0 was attributed to Sb^{III}-O, in accordance with the initial Sb^{III}-O adsorbed on goethite (Fig. 2a). In the presence of MR-1, Sb^{III}-O was transformed to Sb_2S_3 at 4702 eV (Fig. 2a). Linear combination fitting (LCF) of XANES spectra further confirmed that 36 ± 4 % Sb_2S_3 were formed in MR-1+Goe-Sb^{III}+S^0, whereas the proportion of Sb_2S_3 in Goe-Sb^{III}+S^0 (5 ± 2 %) was negligible (Table S-4). In addition, approximately 51 ± 1 % and 39 ± 2 % Sb^{III}-O were oxidised to antimonate (Sb^V-O) in Goe-Sb^{III}+S^0 and MR-1+Goe-Sb^{III}+S^0, respectively (Fig. 2a and Table S-4). The abiotic oxidation was ascribed to the electron transfer between Sb^{III}-O and goethite (Yin *et al.*, 2021), as detailed in SI.

The mass balance calculations show that 1.52 ± 0.62 μmol Sb^{III}-O were precipitated in the presence of MR-1 at the end of incubation, but 4.30 ± 0.48 μmol Sb as Sb_2S_3 were detected by XANES analysis. The much higher amount of Sb as Sb_2S_3 than the loss of dissolved Sb^{III}-O suggests that not only dissolved, but also adsorbed Sb^{III}-O, reacted with biogenic sulfide to form Sb_2S_3 precipitates. Consistent with this observation, the precipitation of Sb_2S_3 may readily occur in mildly acidic environments, such as paddy soils, wetland, groundwater and lake/river systems where sulfide was commonly less than 10 μM (Figs. 3a, S-6a). Actually, if sulfide or pH slightly increased, instead of Sb_2S_3, soluble thioantimony (Sb-S) would be prevalent (Figs. 3a, S-6a), resulting in enhanced Sb release (Ye *et al.*, 2022).

Unlike our results, a previous study ascribed the immobilisation of Sb to incorporation of Sb^V-O into the newly formed secondary iron phases (*i.e.* feroxyhyte and goethite) (Burton *et al.*, 2019). However, that pathway is not suitable in our system because the phase transformation of goethite was not significant. In detail, Fe XANES LCF analysis suggest that 99 ± 0 % of Fe phases remained as goethite and negligible iron sulfides (1 ± 1 % of total Fe) were formed at the end of incubation (Fig. S-5 and Table S-5). S K-edge XANES also confirmed the negligible formation of iron sulfides (4 ± 1 % of total S; Fig. S-5 and Table S-6). The newly formed iron sulfide may co-precipitate with or re-adsorb Sb, but its low content (1 ± 1 % of total Fe) limited its contribution to Sb mobility (detailed in SI).

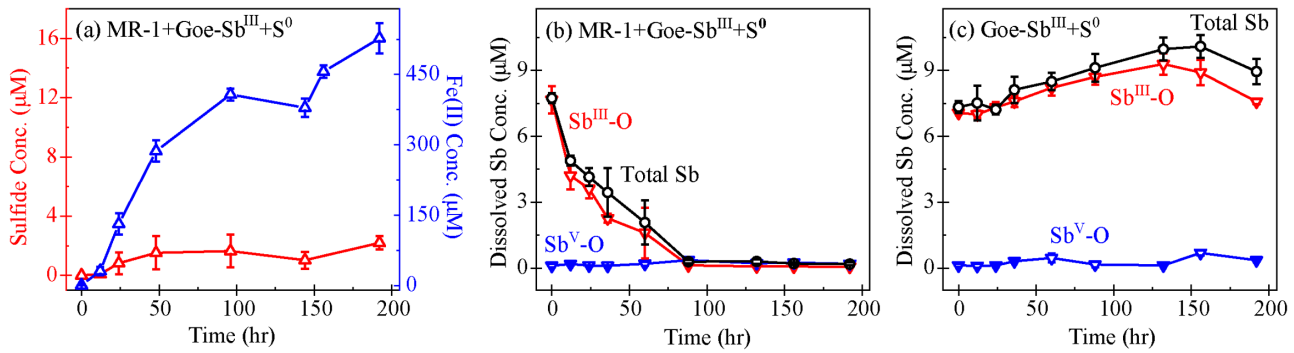

Figure 1 **(a)** Changes in dissolved sulfide (red) and Fe(II) (blue). **(b)** Total dissolved Sb (black), Sb^{III}-O (red), and Sb^V-O (blue) during incubation in MR-1+Goe-Sb^{III}+S^0 at pH 6.5. **(c)** Changes in dissolved Sb species in abiotic control Goe-Sb^{III}+S^0. Fe(II) and sulfide were not detected in Goe-Sb^{III}+S^0.

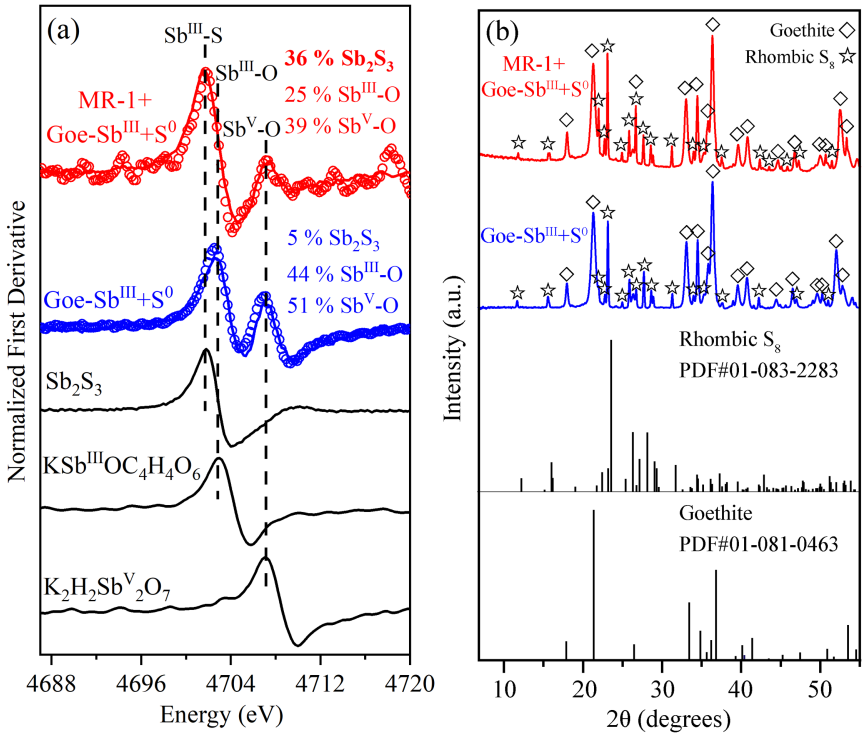

Figure 2 **(a)** Observed (circles) and linear combination fitting (lines) for the first derivative of normalised Sb L_I-edge XANES for samples at the end of incubation. Spectra for standard references are also shown for comparison. The results of linear combination fitting analysis are shown in Table S-4. **(b)** Synchrotron X-ray powder diffraction pattern recorded from the solid in MR-1+Goe-Sb^{III}+S^0 and Goe-Sb^{III}+S^0 at the end of incubation.

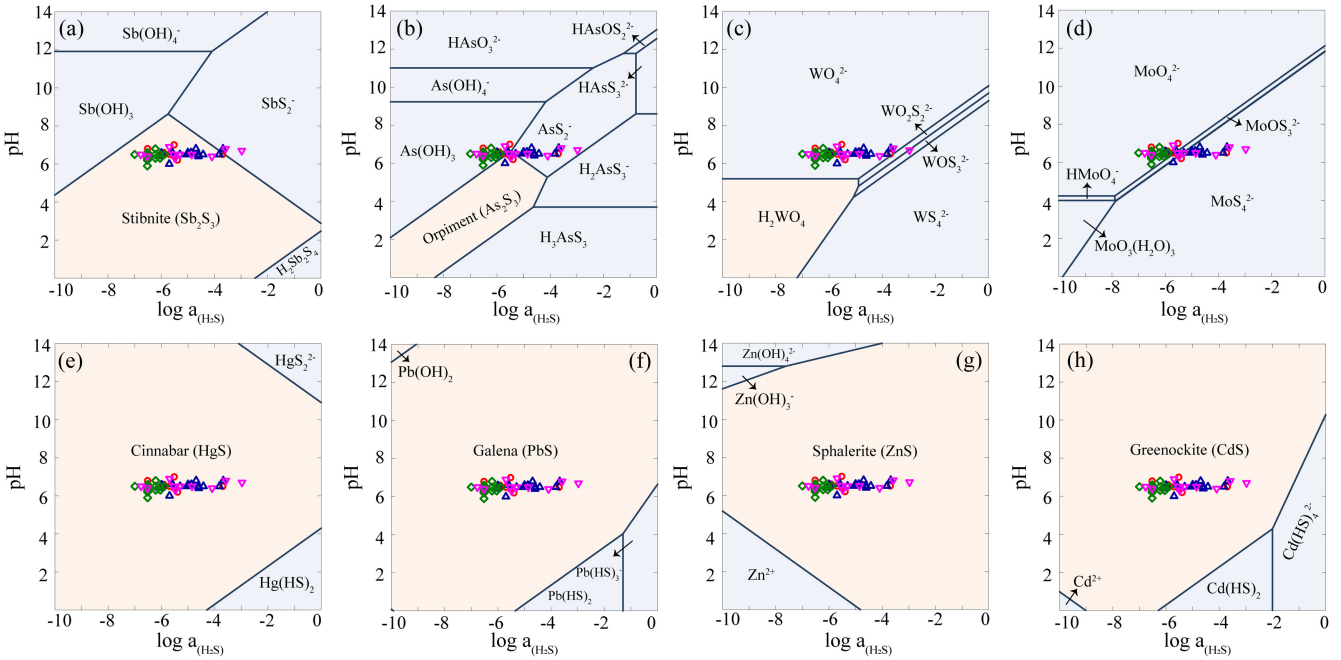

Figure 3 Species of **(a)** Sb, **(b)** As, **(c)** W, **(d)** Mo, **(e)** Hg, **(f)** Pb, **(g)** Zn and **(h)** Cd in the reaction with different log activity (H_2S) and pH values in the presence of goethite at 25 °C. The activities of these metal(loid)s were set as 10 μM. The red, blue, green and magenta symbols represent the sulfide concentrations in mildly acidic paddy, wetland, groundwater and lake/river systems, respectively. The data are from references in Table S-7.

In addition, synchrotron X-ray diffraction (SXRD) did not resolve new Fe minerals other than goethite and rhombic S_8 in both Goe-Sb^{III}+S^0 and MR-1+Goe-Sb^{III}+S^0 samples at the end of incubation (Fig. 2b).

A recent study demonstrated that Sb^V-O can readily incorporate into the goethite structure during Fe(II) catalysed recrystallisation without phase transformation (Burton *et al.*, 2020). This phenomenon, which involves relatively rapid

interactions between goethite and Fe(II), may have contributed to the immobilisation of Sb under our experimental conditions. However, an assessment of the quantitative contribution of Fe(II)-induced goethite recrystallisation to Sb immobilisation in our experiment is beyond the scope of the present study. Despite this possible uncertainty, it is clear from our results that a substantial amount of Sb was certainly immobilised *via* Sb_2S_3 precipitation due to the IRB-driven S^0 reduction.

Strong impacts from weak S^0 reduction on metal(loid)s mobility. Since environmental acidification is inevitable with increasing CO_2 emission (Terhaar *et al.*, 2020), the effect of marginal S^0 reduction under mildly acidic conditions should be paid more attention. This effect can be extended to other metal(loid)s including arsenic, tungsten, molybdenum, mercury, lead, zinc and cadmium. To justify the proposition, reaction path modelling was performed to predict the speciation change of these metal(loid)s at 10 μM (Fig. 3) and 1 μM (Fig. S-6) as a function of pH and the activity of sulfide. As shown in our thermodynamic calculations (Figs. 3b-d, S-6b-d), soluble thiolated species such as thioarsenic (As-S), thiotungsten (W-S), and thiomolybdenum (Mo-S) would occur in multiple low sulfide (<0.1 mM) environments. Consistent with our results, As-S has been detected in paddy soil porewaters when sulfide <10 μM at pH 6.5, and the As-S formation was promoted by S^0 (Wang *et al.*, 2020). In general, the formation of As-S and W-S may enhance their mobility (Mohajerin *et al.*, 2014; Ye *et al.*, 2020), whereas Mo-S is less mobile than Mo-O due to its higher affinity for sulfide minerals and natural organic matter (Smedley and Kinniburgh, 2017).

On the other hand, S^0 reduction leads to precipitation of sulfide minerals, such as cinnabar (HgS), galena (PbS), sphalerite (ZnS), and greenockite (CdS) (Figs. 3e-h, S-6e-h). These minerals immobilise metal(loid)s due to minor S^0 reduction (~10 μM), resulting in decoupling of Fe(II) and metal(loid)s release to the aqueous phase during the microbial Fe(III) reduction. However, most previous studies attributed the decoupling of Fe(II) and metal(loid)s release to re-adsorption on, or incorporation into, the newly formed iron minerals (Hockmann *et al.*, 2020). This study provides a new perspective that IRB shape the mobility and transformation of metal(loid)s *via* S^0 respiration. Even under mildly acidic conditions where Fe(III) reduction is prevailing, the underappreciated and marginal S^0 reduction plays a vital role in the mobility of metal(loid)s.

Author Contributions

LY conceived the study, performed the experiments, interpreted the data and wrote the first draft; CJ contributed to the work design, data interpretation and manuscript revision.

Competing interests:

The authors declare no competing financial interest.

Acknowledgements

We acknowledge the financial support of the National Natural Science Foundation of China (41877378 and 41425016), the China Postdoctoral Science Foundation (2021M691924), and the Natural Science Foundation of Shandong Province, China (ZR2020ZD34, ZR2021QD054).

Editor: Andreas Kappler

Additional Information

Supplementary Information accompanies this letter at https://www.geochemicalperspectivesletters.org/article2215.

Cite this letter as: Ye, L., Jing, C. (2022) Iron(III) reducing bacteria immobilise antimonite by respiring elemental sulfur. *Geochem. Persp. Let.* 21, 37–41. https://doi.org/10.7185/geochemlet.2215

References

Burton, E.D., Bush, R.T., Sullivan, L.A., Hocking, R.K., Mitchell, D.R.G., Johnston, S.G., Fitzpatrick, R.W., Raven, M., McClure, S., Jang, L.Y. (2009) Iron-monosulfide oxidation in natural sediments: Resolving microbially mediated S transformations using XANES, electron microscopy, and selective extractions. *Environmental Science & Technology* 43, 3128–3134. https://doi.org/10.1021/es8036548

Burton, E.D., Bush, R.T., Johnston, S.G., Sullivan, L.A., Keene, A.F. (2011) Sulfur biogeochemical cycling and novel Fe-S mineralization pathways in a tidally re-flooded wetland. *Geochimica et Cosmochimica Acta* 75, 3434–3451. https://doi.org/10.1016/j.gca.2011.03.020

Burton, E.D., Hockmann, K., Karimian, N., Johnston, S.G. (2019) Antimony mobility in reducing environments: The effect of microbial iron(III)-reduction and associated secondary mineralization. *Geochimica et Cosmochimica Acta* 245, 278–289. https://doi.org/10.1016/j.gca.2018.11.005

Burton, E.D., Hockmann, K., Karimian, N. (2020) Antimony sorption to goethite: Effects of Fe(II)-catalyzed recrystallization. *ACS Earth and Space Chemistry* 4, 476–487. https://doi.org/10.1021/acsearthspacechem.0c00013

Cummings, D.E., March, A.W., Bostick, B., Spring, S., Caccavo, F., Fendorf, S., Rosenzweig, R.F. (2000) Evidence for microbial Fe(III) reduction in anoxic, mining-impacted lake sediments (Lake Coeur d'Alene, Idaho). *Applied and Environmental Microbiology* 66, 154–162. https://doi.org/10.1128/AEM.66.1.154-162.2000

Flynn, T.M., O'Loughlin, E.J., Mishra, B., DiChristina, T.J., Kemner, K.M. (2014) Sulfur-mediated electron shuttling during bacterial iron reduction. *Science* 344, 1039–1042. https://doi.org/10.1126/science.1252066

Helz, G.R. (2021) Dissolved molybdenum asymptotes in sulfidic waters. *Geochemical Perspectives Letters* 19, 23–26. https://doi.org/10.7185/geochemlet.2129

Hockmann, K., Lenz, M., Tandy, S., Nachtegaal, M., Janousch, M., Schulin, R. (2014) Release of antimony from contaminated soil induced by redox changes. *Journal of Hazardous Materials* 275, 215–221. https://doi.org/10.1016/j.jhazmat.2014.04.065

Hockmann, K., Tandy, S., Lenz, M., Reiser, R., Conesa, H.M., Keller, M., Studer, B., Schulin, R. (2015) Antimony retention and release from drained and waterlogged shooting range soil under field conditions. *Chemosphere* 134, 536–543. https://doi.org/10.1016/j.chemosphere.2014.12.020

Hockmann, K., Planer-Friedrich, B., Johnston, S.G., Peiffer, S., Burton, E.D. (2020) Antimony mobility in sulfidic systems: Coupling with sulfide-induced iron oxide transformations. *Geochimica et Cosmochimica Acta* 282, 276–296. https://doi.org/10.1016/j.gca.2020.05.024

Kappler, A., Bryce, C., Mansor, M., Lueder, U., Byrne, J.M., Swanner, E.D. (2021) An evolving view on biogeochemical cycling of iron. *Nature Reviews Microbiology* 19, 2679–2698. https://doi.org/10.1038/s41579-020-00502-7

Karimian, N., Johnston, S.G., Burton, E.D. (2018) Iron and sulfur cycling in acid sulfate soil wetlands under dynamic redox conditions: A review. *Chemosphere* 197, 803–816. https://doi.org/10.1016/j.chemosphere.2018.01.096

Kontny, A., Schneider, M., Eiche, E., Stopelli, E., Glodowska, M., Rathi, B., Göttlicher, J., Byrne, J.M., Kappler, A., Berg, M., Thi, D.V., Trang, P.T. K., Viet, P.H., Neumann, T. (2021) Iron mineral transformations and their

impact on As (im)mobilization at redox interfaces in As-contaminated aquifers. *Geochimica et Cosmochimica Acta* 296, 189–209. https://doi.org/10.1016/j.gca.2020.12.029

Mohajerin, T.J., Helz, G.R., White, C.D., Johannesson, K.H. (2014) Tungsten speciation in sulfidic waters: Determination of thiotungstate formation constants and modeling their distribution in natural waters. *Geochimica et Cosmochimica Acta* 144, 157–172. https://doi.org/10.1016/j.gca.2014.08.037

Peiffer, S., Kappler, A., Haderlein, S.B., Schmidt, C., Byrne, J.M., Kleindienst, S., Vogt, C., Richnow, H.H., Obst, M., Angenent, L.T., Bryce, C., McCammon, C., Planer-Friedrich, B. (2021) A biogeochemical–hydrological framework for the role of redox-active compounds in aquatic systems. *Nature Geoscience* 14, 264–272. https://doi.org/10.1038/s41561-021-00742-z

Planer-Friedrich, B., Forberg, J., Lohmayer, R., Kerl, C.F., Boeing, F., Kaasalainen, H., Stefánsson, A. (2020) Relative abundance of thiolated species of As, Mo, W, and Sb in hot springs of Yellowstone National Park and Iceland. *Environmental Science & Technology* 54, 4295–4304. https://doi.org/10.1021/acs.est.0c00668

Poulton, S.W., Krom, M.D., Raiswell, R. (2004) A revised scheme for the reactivity of iron (oxyhydr)oxide minerals towards dissolved sulfide. *Geochimica et Cosmochimica Acta* 68, 3703–3715. https://doi.org/10.1016/j.gca.2004.03.012

Smedley, P.L., Kinniburgh, D.G. (2017) Molybdenum in natural waters: A review of occurrence, distributions and controls. *Applied Geochemistry* 84, 387–432. https://doi.org/10.1016/j.apgeochem.2017.05.008

Sun, W., Xiao, T., Sun, M., Dong, Y., Ning, Z., Xiao, E., Tang, S., Li, J. (2015) Diversity of the sediment microbial community in the Aha watershed (southwest China) in response to acid mine drainage pollution gradients. *Applied and Environmental Microbiology* 81, 4874–4884. https://doi.org/10.1128/AEM.00935-15

Terhaar, J., Kwiatkowski, L., Bopp, L. (2020) Emergent constraint on Arctic Ocean acidification in the twenty-first century. *Nature* 582, 379–383. https://doi.org/10.1038/s41586-020-2360-3

Wang, J., Shaheen, S.M., Jing, M., Anderson, C.W.N., Swertz, A.-C., Wang, S.-L., Feng, X., Rinklebe, J. (2021) Mobilization, methylation, and demethylation of mercury in a paddy soil under systematic redox changes. *Environmental Science & Technology* 55, 10133–10141. https://doi.org/10.1021/acs.est.0c07321

Wang, J.J., Kerl, C.F., Hu, P.J., Martin, M., Mu, T.T., Bruggenwirth, L., Wu, G.M., Said-Pullicino, D., Romani, M., Wu, L.H., Planer-Friedrich, B. (2020) Thiolated arsenic species observed in rice paddy pore waters. *Nature Geoscience* 13, 282–287. https://doi.org/10.1038/s41561-020-0533-1

Ye, L., Meng, X., Jing, C. (2020) Influence of sulfur on the mobility of arsenic and antimony during oxic-anoxic cycles: Differences and competition. *Geochimica et Cosmochimica Acta* 288, 51–67. https://doi.org/10.1016/j.gca.2020.08.007

Ye, L., Zhong, W., Zhang, M., Jing, C. (2022) New mobilization pathway of antimonite: thiolation and oxidation by dissimilatory metal-reducing bacteria via elemental sulfur respiration. *Environmental Science & Technology* 56, 652–659. https://doi.org/10.1021/acs.est.1c05206

Yin, X.L., Zhang, G.Q., Su, R., Zeng, X.F., Yan, Z.L., Zhang, D.N., Ma, X., Lei, L., Lin, J.R., Wang, S.F., Jia, Y.F. (2021) Oxidation and incorporation of adsorbed antimonite during iron(II)-catalyzed recrystallization of ferrihydrite. *Science of The Total Environment* 778, 146424. https://doi.org/10.1016/j.scitotenv.2021.146424

Zhou, Z., Muehe, E.M., Tomaszewski, E., Lezama Pacheco, J., Kappler, A., Byrne, J.M. (2020) Effect of natural organic matter on the fate of cadmium during microbial ferrihydrite reduction. *Environmental Science & Technology* 54, 9445–9453. https://doi.org/10.1021/acs.est.0c03062